Discrete Estimation of Data Completeness for 3D Scan Trajectories with Detector Offset

Andreas Maier[1], Patrick Kugler[2], Günter Lauritsch[2], Joachim Hornegger[1]

[1]Pattern Recognition Lab and SAOT Erlangen, FAU Erlangen
[2]Siemens AG, Healthcare, Forchheim
andreas.maier@fau.de

Abstract. The sequence of source and detector positions in a CT scan determines reconstructable volume and data completeness. Commonly this is regarded already in the design phase of a scanner. Modern flat-panel scanners, however, allow to acquire a broad range of positions. This enables many possibilities for different scan paths. However, every new path or trajectory implies different data completeness. Analytic solutions are either designed for special trajectories like the Tam-window for helical CT scans or do not incorporate the actual detector size such as Tuy's condition.
In this paper, we describe a method to determine the voxel-wise data completeness in percent for discretely sampled trajectories. Doing so, we are able to model any sequence of source and detector positions. Using this method, we are able to confirm known theory such as Tuy's condition and data completeness of trajectories using detector offset to increase the field-of-view. As we do not require an analytic formulation of the trajectory, the algorithm will also be applicable to any other source-detector-path or set of source-detector-path segments.

1 Introduction

Modern flat-panel CT scanners allow many scan configurations. In particular, multi-axis C-arm systems allow a broad range of application scenarios. For example, Herbst et al. identified novel opportunities to reduce the scan range for eliptical fields-of-view [1] and Xia et al. found that reduction of scan range and dose is possible for volume-of-interest scans [2]. Both studies, however, demonstrate these effects only in 2D imaging geometries and lack the analysis in 3D.

While the adjustment of the scan configuration for a specific task allows many different benefits ranging from image quality improvement [3] to novel applications such as long-volume imaging [4], data completeness is typically determined for each scan configuration analytically. This results in new analytic formulations for each new path. Important examples are Tuy's condition [5] and the Tam-window for helical scans [6]. While Tuy's condition holds for any cone-beam scan, it does not incorporate detector size and delivers thus a necessary but not sufficient condition. Tam's window applies only for helical scans.

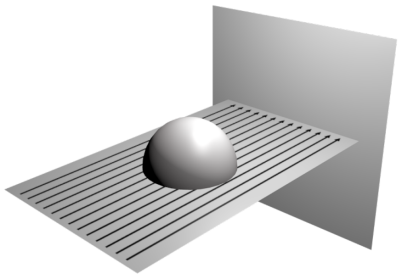

Fig. 1. While X-rays form integrals along individual rays (denoted as arrows), the 3D Radon transform evaluates plane integrals. Note that an integral along a line on the 2D X-ray detector evaluates exactly a plane integral in parallel geometry.

Thus, there is a need for a method to compute data completeness for arbitrary trajectories. In the following, we describe such a method for discrete source and detector positions. Note that the method is conceptually very close previously published methods [7,8] which have not been applied to off-center detector trajectories to the knowledge of the authors.

2 3D Radon Space

While 2D Radon transform and 2D X-ray transform are identical, the 3D Radon transform differs from the 3D X-ray transform [5]. Figure 1 shows this difference in a parallel geometry: The line integrals obtained by X-rays are indicated as arrows. The respective plane integral in 3D Radon space is obtained as line integral on the 2D X-ray detector at the intersection of the plane and the detector. Note that we assume that the object fits completely onto the X-ray detector.

For cone-beam geometries, the above relation is not entirely correct. The line integral on the 2D projector is not identical to a plane integral in object space as the rays generally form fans through the object. The fan integral is weighted with increasing magnification though the object [5]. While this is important for the reconstruction algorithm, it does not affect data completeness in general.

3 Point-wise Data Completeness in Cone-beam Geometry

We know that we are able to reconstruct the object of interest, if the 3D Radon data is completely acquired. In order to compute a local approximation of the amount of acquired Radon data, we investigate the coverage of Radon planes for every voxel. In order to do so, we investigate 3D coverage of Radon plane normals on a unit sphere, called Radon sphere in the following. In this context, we ignore object-dependent information such as truncation on the detector. Note that this formalism still allows to include the detector size into the data completeness estimation. Figure 2 shows this process for a circular trajectory. In fact,

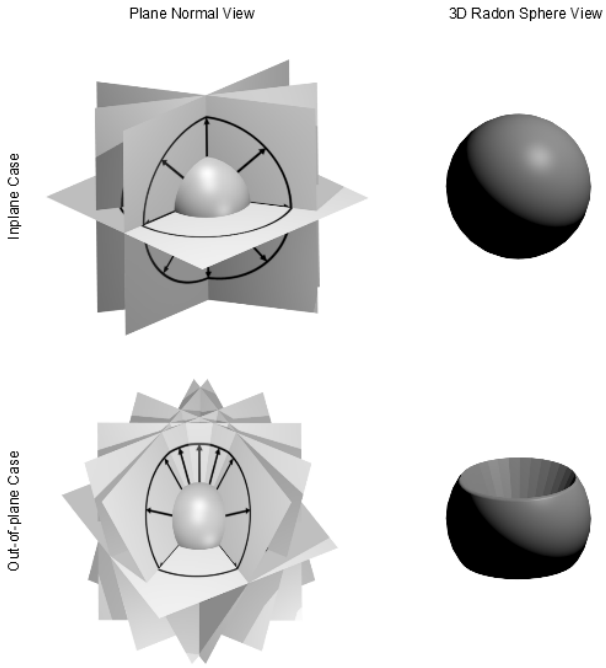

Fig. 2. Example for 3D Radon space sampling for a point of interest for a circular scan trajectory: The upper row shows the sampling for a point inside the acquisition plane. The normals of the Radon planes (denoted as arrows) that are measured lie on a plane that is aligned with the rotation axis for each projection image. By rotation, the entire Radon sphere is sampled. In the bottom row, a case is shown where the point of interest is below the reconstruction plane. In this case, the plane normals lie in a plane that is slant with respect to the rotation axis. Thus rotation misses planes aligned with the rotation axis. This leads to an incomplete sampling of the Radon sphere.

the requirement of complete sampling of the radon sphere is identical to Tuy's condition as Tuy postulates that every plane that intersects the object needs to intersect the source path. Given a detector that fits the entire object, this allows to compute the respective plane integral, because we are able to compute the respective line integral on the 2D detector. Thus if all planes that intersect the object also intersect the source trajectory, all plane integrals are measured and the Radon sphere is sampled completely at every point of the object.

4 Numerical Data Completeness Estimation

So far we have only summarized known theory for data completeness and showed the relation between Tuy's condition and the Radon sphere sampling. As mentioned above, Tuy's condition does not incorporate the actual detector size. In

order to include this in our algorithm, we now determine the Radon sphere sampling at every voxel position in the volume under consideration.

First, we require a discrete sampling of the unit sphere in vectors $\boldsymbol{u}$. Here, we follow ideas of Saff et al. [9]. We approximate the unit sphere in intervals of the same angular step size $\Delta\theta$. For the elevation angle α, we sample the range $[-\pi/2, \pi/2]$ in steps of $\Delta\theta$ size. For the azimuth angle β, we determine a step size $\Delta\beta$ that is dependent on the elevation angle α:

$$\Delta\beta = \sin^{-1}\left(\frac{\sin(\Delta\theta/2)}{\cos\,\alpha}\right) * 2$$

Note that it is sufficient to sample only half of the unit sphere, as the plane integrals are symmetric for top and bottom (cf Figure 2). In the following, we denote the total number of points sampled on the sphere as N_u.

Next, we need to compute the data completeness in terms of Radon sphere coverage for every voxel. We want to identify vectors of the unit sphere $\boldsymbol{u}$ that are covered by the normal vectors of the Radon planes, i.e. that are perpendicular to the current viewing direction $\boldsymbol{d}$, which is the connection between the source and the current voxel. In the following, we will only consider those vectors $\boldsymbol{d}$ that actually hit the detector.

As the inner product of two unit vectors describes the cosine of the angle between the two vectors and we want to find vectors that deviate less than $\Delta\theta$, the following condition is true for the vectors of interest:

$$|\cos^{-1}(\boldsymbol{d}^\top \boldsymbol{u}) - 90°| < \Delta\theta$$

By rearranging, we remove the expensive trigonometric function:

$$|\boldsymbol{d}^\top \boldsymbol{u}| < \sin\Delta\theta$$

Note that the sine function can be precomputed, as $\Delta\theta$ is a constant in our case. Above equation is evaluated for every unit vector and every viewing direction. The unique number of unit vectors that satisfy the condition above is denoted as N_c in the following.

After evaluation of this condition of every unit vector $\boldsymbol{u}$, we are able to compute a coverage c that gives the coverage of the Radon sphere

$$c = \frac{N_c}{N_u} \cdot 100\,\%.$$

As above process is repeated for every voxel and every projection, the algorithm has a complexity of $\mathcal{O}(N^3 \cdot P \cdot N_u)$, if N^3 is the number of voxels and P the number of projections. Note that P should be sampled at least in angular intervals of $\Delta\theta$ and thus both P and N_u are dependent on this angular sampling, i.e. the smaller $\Delta\theta$ the higher the complexity.

5 Results

We investigated two types of trajectories: Helix scans with the detector centered, i.e. the principal ray passes the rotation axis and hits the detector in the center.

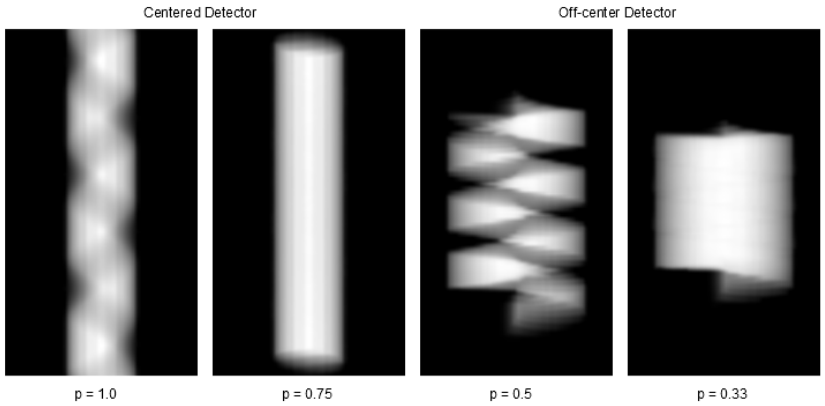

Fig. 3. Integral projections the reconstructable volume for three turns of the helix. With off-center detector, the $p = 0.33$ configuration still lacks a very small amount of data that is moving along the helix.

Furthermore, we investigated a configuration with an off-center detector. Here the configuration was that the principal ray passes the rotation axis and hits the detector at the most left pixel row. We simulated three rotations of the helix at different forward feed along the rotation axis. The detector was in landscape orientation and had a ratio of 4:3. Volumetric sampling was performed on a $64 \times 64 \times 128$ grid. $\Delta\theta$ was set to 1.5°. We denote the forward motion per helical turn as h_{helix}. In order to normalize this independent of the detector size, we define a p value that is motivated by pitch in CT. However, we have to take into account, that perspective projection may magnify the current view in an arbitrary flat-panel system. Therefore, the detector height projected into the iso-center h_{iso} is taken into account. p is then found as $p = \frac{h_{\text{helix}}}{h_{\text{iso}}}$.

For visualization, we set a cut-off value of $c = 90\,\%$ and projected the reconstructable areas of the volume as line integrals to a virtual large detector to display all configurations. The visualizations were created using the CONRAD software framework [10]. Figure 3 shows the results. The center configuration with $p = 1.0$ shows the longest coverage in rotation axis direction, however, there are areas that are not completely covered within the volume. The configuration with $p = 0.75$ delivers a complete coverage of the volume, i.e. there are no gaps in between. This result matches known theory for helical scans [6]. For the off-center cases, the coverage in rotation axis direction is shorter and their pitch values are respectively shorter. However, the field-of-view is almost doubled in inplane orientation. With $p = 0.5$ the off-center configuration is not able to cover a continuous volume. The configuration with $p = 0.33$ is able to cover the entire field-of-view with at least 99 % completeness. However, this comes at a reduction of coverage in axial direction.

6 Discussion and Outlook

We presented an algorithm for the computation of data completeness at every voxel. Conceptually, the algorithm is very close to [7,8]. We show that the algorithm is suited to analyze scan configurations with different detector offset. The results on the helical configuration match the theory known from literature. Furthermore, it is interesting to note, that the off-center configuration is close to complete, but still lacks small amounts of data ($< 1\,\%$). Limitations of the presented method are that it does not handle object truncation and it does not allow to recommend a specific reconstruction algorithm. However, source position and detector size are handled correctly.

Disclaimer. The concepts and information presented in this paper are based on research and are not commercially available.

References

1. Herbst M, Schebesch F, Berger M, Fahrig R, Hornegger J, Maier A. Improved trajectories in C-Arm computed tomography for non-circular fields of view. In: Noo F, editor. Proceedings of the third international conference on image formation in x-ray computed tomography; 2014. p. 274–278.
2. Xia Y, Maier A, Berger M, Hornegger J. Region of Interest Reconstruction from Dose-minimized Super Short Scan Data. In: Springer, editor. Bildverarbeitung für die Medizin 2014; 2014. p. 48–53.
3. Stayman JW, Siewerdsen JH. Task-Based Trajectories in Iteratively Reconstructed Interventional Cone-Beam CT. In: The 12th International Meeting on Fully Three-Dimensional Image Reconstruction in Radiology and Nuclear Medicine; 2013. p. 257–260.
4. Yu Z, Maier A, Schoenborn M, Vogt F, Koehler C, Lauritsch G, et al. Frist experimental results on long-object imaging using a reverse helical trajectory with a C-arm system. In: Frederic N, editor. Proceedings of The second international conference on image formation in x-ray computed tomography; 2012. p. 364–368.
5. Zeng GL. Medical Image Reconstruction. Springer; 2010.
6. Tam KC, Samarasekera S, Sauer F. Exact cone beam CT with a spiral scan. Physics in Medicine and Biology. 1998;43(4):1015.
7. Metzler SD, Bowsher JE, Jaszczak RJ. Geometrical similarities of the Orlov and Tuy sampling criteria and a numerical algorithm for assessing sampling completeness. IEEE Transactions on Nuclear Science. 2003;50:1550–1555.
8. Liu B, Bennett J, Wang G, De Man B, Zeng K, Yin Z, et al. Completeness map evaluation demonstrated with candidate next-generation cardiac CT architectures. Medical physics. 2012;39(5):2405–2416.
9. Saff EB, Kuijlaars ABJ. Distributing many points on a sphere. The Mathematical Intelligencer. 1997;19(1):5–11.
10. Maier A, Hofmann H, Berger M, Fischer P, Schwemmer C, Wu H, et al. CONRAD - A Software Framework for Cone-Beam Imaging in Radiology. Medical Physics. 2013;40(11):111914–1–8.